Progress In Electromagnetics Research C, Vol. 31, 137–151, 2012

DESIGN OF COMPACT LOWPASS FILTER WITH ULTRA-WIDE STOPBAND USING THIN SLOTS

J.-Y. Wu, Y.-H. Tseng, and W.-H. Tu*

Department of Electrical Engineering, National Central University, Jhongli, Taoyuan 32001, Taiwan

Abstract—This paper presents a compact microstrip stepped-impedance lowpass filter with ultra-wide stopband by using back-to-back C-shaped and triple C-shaped thin slots. The properties of several thin slots in the ground plane have been investigated in this paper. With the full-wave simulation results and a simplified equivalent model, the total equivalent inductance of the thin slots can be extracted at cutoff frequency for lowpass filter design purpose. On the other hand, the thin slots work as bandstop filter at the stopband of the lowpass filter for a better stopband rejection. The proposed lowpass filter with a cutoff frequency of 2 GHz shows a wide stopband with an over 25-dB attenuation up to 17.5 GHz. From dc to 2 GHz, the insertion loss is less than 0.3 dB and the return loss is greater than 20 dB. In comparison to the conventional stepped-impedance lowpass filter with the same passband performance, the proposed lowpass filter shows not only a 24.3% size reduction but also a better stopband rejection.

1. INTRODUCTION

In communication systems, lowpass filters (LPFs) are widely used to suppress high frequency harmonics with the requirements of small circuit size, low insertion loss, wide stopband, and sharp roll-off. Some planar LPFs were reported in [1–6]. In [1], the spurious passband of a conventional stepped-impedance LPF can be suppressed by using asymmetrical microstrip step discontinuity. In [2], the filter uses interdigital structure between the symmetric rectangular couple capacitors, which not only reduce the filter size but also provide the finite attenuation poles to suppress the first spurious passband. A compact wide-stopband LPF using embedding band-stop structure was

Received 26 May 2012, Accepted 16 July 2012, Scheduled 18 July 2012

* Corresponding author: Wen-Hua Tu (whtu@ee.ncu.edu.tw).

designed in [3]. A microstrip elliptic-function LPF using a microstrip line section in parallel with an interdigital capacitor was proposed in [4]. To achieve wider stopband, stepped-impedance resonators (SIRs) are usually employed or loaded in the circuit designs. In [5], the compact LPF with ultra-wide stopband is designed with SIRs and open-circuited stubs. A circular hairpin resonator integrated with SIR was proposed in [6]. By the loaded SIRs, transmission zeros can be easily introduced and controlled to suppress the spurious responses. Defected ground structure (DGS) is also widely used in LPF design recently [7–18]. In [8], the LPF with cross-shape DGS shows a 20-dB suppression from 4.25 GHz to 15.9 GHz. In [9], the multilayer LPF is designed based on arrow-shaped DGS with centered etched ellipse. The LPF in [10] is realized by using a cascading microstrip coupled-line hairpin unit, semi-circle DGS and semi-circle stepped-impedance shunt stub. In [12], the proposed LPF featuring sharp cut-off response, 100 dB/GHz, consists of the stepped-impedance hairpin resonator, an improved split-ring resonator defected ground structure and elliptical DGSs. In [13], two quasi-elliptic LPFs with interdigital DGS are proposed. In [14], a novel elliptic-function LPF consisting of a dumb-bell-shaped DGS, a spiral-shaped DGS and a broadened microstrip line is presented. The LPF with Hilbert curve ring DGS achieves high out-band suppression of more than 33 dB [15]. Furthermore, the compact LPF in [16] is demonstrated by employing meandered slotted-grounded-plane resonator to obtain wide rejection bandwidth and high attenuation rate.

In this paper, a compact microstrip stepped-impedance lowpass filter (SI-LPF) with ultra-wide stopband by using back-to-back C-shaped and triple C-shaped thin slots is presented. In Section 2, the equivalent circuit of the thin slot is outlined. In Section 3, the properties of different thin slots are investigated and discussed. In Sections 4 and 5, two proposed LPFs using thin slots and a conventional stepped-impedance LPF for comparison purpose were designed, fabricated and measured. In comparison to previous works, the proposed LPF shows the advantages of compactness, relaxed fabrication tolerance, and better stopband rejection level.

2. THE EQUIVALENT MODEL OF THIN SLOT

Figure 1(a) shows a microstrip line with a thin slot aperture on its ground plane. The circuit is built on a 0.508-mm RT/Duroid 5880 substrate with the relative dielectric constant of 2.2 and a loss tangent of 0.0012. It should be noted that all the circuits in this paper use this substrate. The parameters are: $W_h = 0.2\,\text{mm}$, $W_s = 0.2\,\text{mm}$,

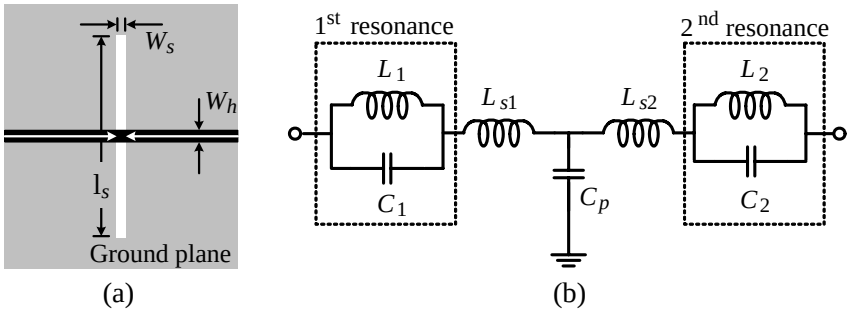

Figure 1. A thin slot (a) configuration, (b) equivalent circuit.

and $l_s = 30\,\text{mm}$. Figure 1(b) shows the equivalent model of a thin slot, which consists of two parallel LC tanks and a π model. The equivalent model parameters can be calculated as [18]

$$C_i = \frac{1}{Z_0} \cdot \frac{1}{4\pi\Delta f_{3\,\text{dB}\_i}} \tag{1a}$$

$$L_i = \frac{1}{(2\pi f_{0i})^2 C_i} \quad \text{for} \quad i = 1, 2 \tag{1b}$$

$$C_p = -\frac{1}{2\pi\Delta f_T X_{21}} \tag{1c}$$

$$L_{si} = \frac{X_{ii} - X_{21}}{2\pi f_T} + \frac{L_i}{\left(\frac{f_T}{f_{0i}}\right)^2 - 1} \quad \text{for} \quad i = 1, 2 \tag{1d}$$

where Z_0 is the characteristic impedance of the microstrip line, f_{0i} is the i-th resonant frequency, $\Delta f_{3\,\text{dB}\_i}$ is the 3-dB bandwidth at f_{0i}, f_T is the transit frequency when the signal loss smallest, and X_{11}, X_{22}, and X_{21} are the imaginary parts of the three Z-parameters at f_T. The equivalent circuit parameters are: $L_1 = 2.3849\,\text{nH}$, $C_1 = 0.6217\,\text{pF}$, $L_{s1} = 0.7555\,\text{nH}$, $C_p = 6.0494\,\text{fF}$, $L_{s2} = -0.5138\,\text{nH}$, $L_2 = 0.2825\,\text{nH}$, and $C_2 = 0.5684\,\text{pF}$, which can be obtained based on the EM simulated results that are carried out by IE3D [19]. The reference plane is set right above the edge of the thin slot as the two white arrows indicate.

For conventional LPFs using distributed transmission lines, the transmission lines are modeled as series inductors or shunt capacitors at the cutoff frequency. The equivalent model in Figure 1(b) is a wide-band model, and it can fit up to the second resonant frequency of the thin slot. Therefore, this model is especially useful for controlling the stopband performance of a LPF. For the passband design, it provides more than one needs when the transmission lines are modeled as lumped elements at the cutoff frequency that is lower than the first

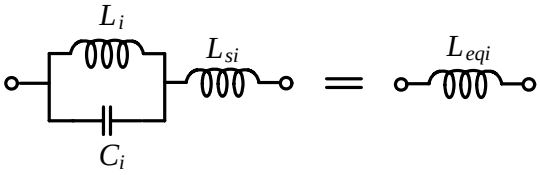

Figure 2. Illustration of the equivalence between an L-C parallel tank with a series inductor and an equivalent series inductor at cutoff frequency.

and second resonant frequencies of a thin slot. To facilitate the LPF design, it is convenient to model a thin slot as an inductor at the cutoff frequency. First, the shunt capacitor C_p with a small capacitance can be ignored at cutoff frequency. Secondly, the parallel L-C tank in series with the series inductor L_S are equivalent to a series inductor In Figure 2, when the $ABCD$ matrices of their corresponding network parameters are equal at cutoff frequency the L_{eqi} can be extracted by

$$L_{eqi} = \frac{L_i}{1 - \omega_c^2 L_i C_i} + L_{si} \quad \text{for} \quad i = 1, 2 \tag{2}$$

where ω_c is the angular cutoff frequency. Thus, we have equivalent inductance $L_{eq1} = 3.8695\,\text{nH}$ and $L_{eq2} = 0.224\,\text{nH}$. In summary, within the passband, the thin slot can be modeled as an inductor, and the total equivalent inductance at cutoff frequency can be extracted by

$$L_{eq} = \frac{L_1}{1 - \omega_c^2 L_1 C_1} + \frac{L_2}{1 - \omega_c^2 L_2 \mathrm{C}_2} + L_{s1} + L_{s2} \tag{3}$$

3. THE PROPERTIES OF THIN SLOT

In order to further investigate and compare the properties of thin slots, in this section, several thin slot layouts as shown in Figure 3 are discussed. The areas of the thin slots are the same ($l = 5\,\text{mm}$ and $W = 5\,\text{mm}$). They are under a high-impedance microstrip line ($Z = 136\,\text{ohm}$ and width $= 0.2\,\text{mm}$). The dimensions of the thin slot are: $l_{sa} = 1.7\,\text{mm}$, $l_{sb} = 1.95\,\text{mm}$, $W_{sa} = 0.2\,\text{mm}$, and gap $= 0.2\,\text{mm}$. The corresponding EM simulations of the four cases are seen in Figure 4. With the EM simulation results, one can follow the extraction procedure in Section 2 to obtain the equivalent model parameters of the slots under study. They are summarized in Table 1. There are three main aspects for the choice of different types of slots: the first resonant frequency, the equivalent inductance, and the 10-dB

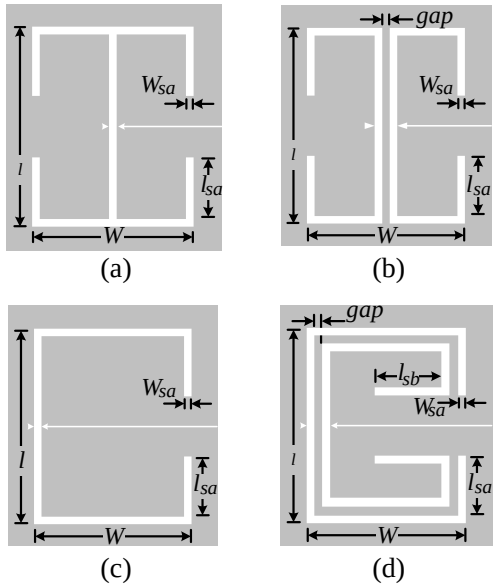

Figure 3. Schematics of thin slots with various shapes in the same area ($l = 5\,\text{mm}$, $W = 5\,\text{mm}$), (a) I-shaped, (b) back-to-back C-shaped, (c) C-shaped, and (d) double C-shaped.

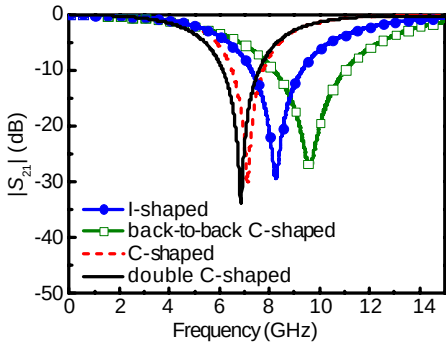

Figure 4. Simulated $|S_{21}|$ of the four thin slots.

suppression bandwidth. It shows that the double C-shaped thin slot has the lowest resonant frequency of 6.86 GHz while the back-to-back C-shaped thin slot has the highest resonant frequency 9.6 GHz. The C-shaped thin slot has the smallest equivalent inductance and the $\Delta f_{10\,\text{dB}}$ suppression bandwidth. This problem can be alleviated by cascading

Table 1. Equivalent circuit parameters and 10-dB bandwidth of four thin slots.

Shape	L_1 (nH)	C_1 (pF)	L_{s1} (nH)	C_p (fF)	L_{s2} (nH)	L_2 (nH)	C_2 (pF)	L_{eq} (nH)	$\Delta f_{10\,\mathrm{dB}}$ (GHz)
I	1.372	0.273	0.196	6.721	-0.075	0.039	0.622	1.619	2.06
B-BC	1.319	0.21	0.469	20.46	-0.201	0.152	0.15	1.801	2.85
C	1.137	0.442	-0.424	6.832	0.476	0.147	0.37	1.44	1.25
D C	1.388	0.389	-1.14	9.517	1.078	0.194	0.273	1.651	1.44

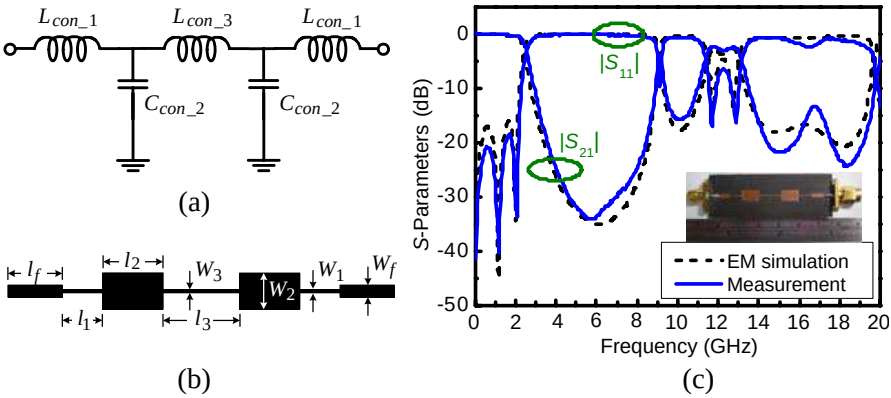

Figure 5. The five-pole conventional SI-LPF (a) prototype, (b) layout, and (c) simulated and measured results.

more thin slots as the double C-shaped shows. In summary, given a fixed circuit size, the I-shaped and the back-to-back C-shaped thin slots are suitable for wideband and high-frequency suppression, while the C-shaped (or double C-shaped) thin slot is good at narrowband and low-frequency suppression.

4. SI-LPF WITH I-SHAPED THIN SLOT

In this section, an improved SI-LPF using I-shaped thin slots is introduced to show the advantages of the proposed LPF. For comparison purpose, we also designed and fabricated a conventional SI-LPF as shown in Figure 5. According to [20], the element values of a Chebyshev five-pole SI-LPF with its cutoff frequency $f_c = 2\,\mathrm{GHz}$ and passband ripple $= 0.1\,\mathrm{dB}$ can be found. The element values are: $L_{con\_1} = 4.6\,\mathrm{nH}$, $C_{con\_2} = 2.2\,\mathrm{pF}$, and $L_{con\_3} = 7.9\,\mathrm{nH}$. Therefore, the

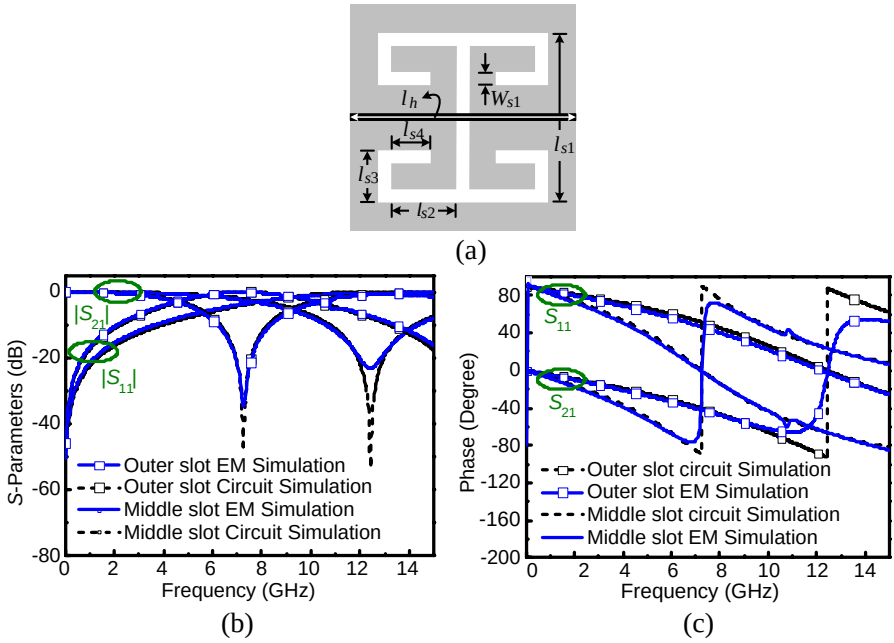

Figure 6. The middle and the outer I-shaped thin slots (a) configuration, (b) magnitude of S-parameters, and (c) phase of S-parameters.

initial dimensions of the conventional SI-LPF are: $l_1 = 7.8\,\text{mm}$, $l_2 = 10.14\,\text{mm}$, $l_3 = 14.5\,\text{mm}$, $W_1 = W_3 = 0.2\,\text{mm}$, $W_2 = 5\,\text{mm}$, $W_f = 1.6\,\text{mm}$ for a 50-ohm line, and $l_f = 10\,\text{mm}$ for convenience. Then, to take the discontinuities and the parasitic effect into consideration, the EM simulator is used to optimize the dimensions: $l_1 = 6.8\,\text{mm}$, $l_2 = 8.1\,\text{mm}$, $l_3 = 11\,\text{mm}$, $W_1 = W_3 = 0.2\,\text{mm}$, and $W_2 = 5\,\text{mm}$. The EM simulated results agree well with the measured results. The size of the conventional SI-LPF is $40.8\,\text{mm} \times 5\,\text{mm}$. The filter exhibits an insertion loss of less than 0.3 dB and a return loss of greater than 18 dB from dc to 2 GHz. As expected, it should be noted that there are spurious passbands at 9.13 GHz and 12.25 GHz due to the distributed characteristic of microstrip line.

To improve the performance of the conventional SI-LPF, by using I-shaped thin slots as show in Figure 6, we propose an improved SI-LPF as shown in Figure 7. In contrast to the conventional SI-LPF, there are three I-shaped thin slots introduced under the three high-impedance narrow-width microstrip lines. For symmetry, the outer two I-shaped slots are identical. The dimensions of the outer I-shaped thin slot are: $l_{s1} = 5\,\text{mm}$, $l_{s2} = 0.875\,\text{mm}$, $l_{s3} = 1.225\,\text{mm}$, $l_{s4} = 0\,\text{mm}$, and

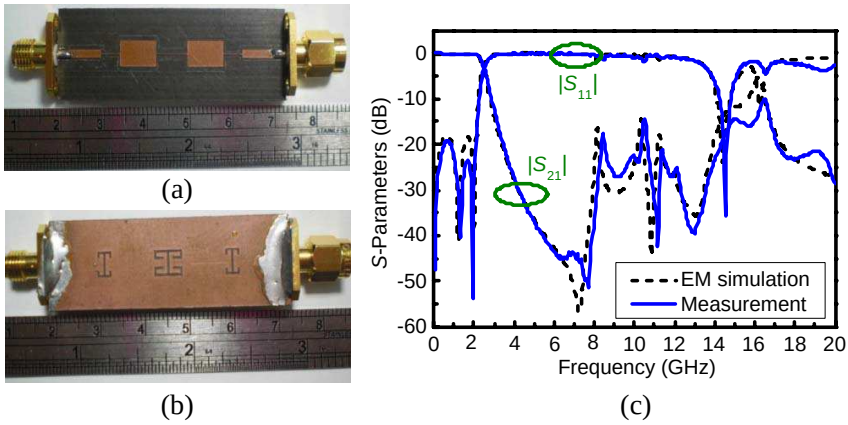

Figure 7. The SI-LPF with I-shaped thin slots, (a) top view, and (b) bottom view, and (c) simulated and measured results.

$W_{s1} = 0.4\,\text{mm}$. We can obtain the equivalent circuit parameters of the outer I-shaped thin slots by (1). The equivalent circuit parameters are: $L_1 = 1.0885\,\text{nH}$, $C_1 = 0.17074\,\text{pF}$, $L_{s1} = 0.27623\,\text{nH}$, $C_p = 11.447\,\text{fF}$, $L_{s2} = -0.07249\,\text{nH}$, $L_2 = 0.067048\,\text{nH}$, and $C_2 = 0.12664\,\text{pF}$. By (3), the total equivalent inductance of the outer I-shaped thin slot at cutoff frequency is $L_{eq} = 1.3836\,\text{nH}$. According to [20] the initial high-impedance lines of length $l_h = 5.4\,\text{mm}$ and width of 0.2 mm is used to realize the rest inductance of $L_{con\_1} - 1.3836 = 3.2164\,\text{nH}$. Furthermore, the dimensions of the middle I-shaped thin slot are: $l_{s1} = 5\,\text{mm}$, $l_{s2} = 2.4\,\text{mm}$, $l_{s3} = 1.7\,\text{mm}$, $l_{s4} = 1.6\,\text{mm}$, and $W_{s1} = 0.4\,\text{mm}$. Similarly, the equivalent circuit parameters are: $L_1 = 1.9033\,\text{nH}$, $C_1 = 0.25031\,\text{pF}$, $L_{s1} = 0.4664\,\text{nH}$, $C_p = 10.528\,\text{fF}$, $L_{s2} = -0.26517\,\text{nH}$, $L_2 = 0.16001\,\text{nH}$, and $C_2 = 0.2436\,\text{pF}$. By using (3), the total equivalent inductance of the middle I-shaped thin slot at cutoff frequency is $L_{eq} = 2.4209\,\text{nH}$. According to [20], the initial high-impedance line of length $l_h = 9.6\,\text{mm}$ and width of 0.2 mm is used to realize the rest inductance of $L_{con\_3} - 2.4209 = 5.4791\,\text{nH}$. It should be noted that the height of the slots is equal to the width of the low-impedance line. When the thin slots introduce the additional inductance, the length of the high-impedance line can be shortened because there is less inductance to be realized by the high-impedance line. Hence, by using the thin slots, the circuit could be miniaturized. Then, to take the discontinuities and the parasitic effect into consideration, the EM simulator is used to optimize the dimensions: $l_h = 4.2\,\text{mm}$ (right and left), and $l_h = 7.4\,\text{mm}$ (middle). The dimensions of the low-impedance wide microstrip lines are the same as those of the conventional one. Figure 6(b) and Figure 6(c) show the EM simulated and the equivalent

circuit simulated results of the I-shaped thin slots for magnitude response and phase response, respectively. The outer slots have a transmission zero at 12.41 GHz, and the middle slot has a transmission zero at 7.29 GHz. The two frequencies of transmission zeros are set to be near the spurious passband frequencies of the conventional SI-LPF for stopband rejection improvement.

The circuit size of the SI-LPF with I-shaped thin slots is 32.4 mm $\times$ 5 mm. Figure 7(c) shows the EM simulated and measured results of the proposed SI-LPF. As expected, the simulated results agree well with measured results. The proposed filter exhibits an insertion loss of less than 0.3 dB and a return loss of greater than 18 dB from dc to 2 GHz. From 3.1 to 10.3 GHz, the stopband rejection level is greater than 15 dB. In comparison, with the same passband performance, the proposed filter shows a 21% size reduction, a better stopband performance, and a relaxed fabrication tolerance. In conventional SI-LPF design, it should be noted that a narrower width high-impedance microstrip line is preferred for obtaining a better-approximated lumped-element inductor. However, this causes several disadvantages such as fabrication sensitivity, poor power handling capability, and high loss.

5. THE COMPACT SI-LPF WITH THE WIDEST STOPBAND

In this section, another SI-LPF using the thin slots is investigated. To optimize the design, back-to-back C-shaped thin slot is employed as it can provide larger inductance (smaller filter circuit size) and wide stopband bandwidth (good filter stopband performance). Two different back-to-back C-shaped thin slots are used under the outer two high-impedance lines. Furthermore, a triple C-shaped thin slot as shown in Figure 8(a) is used under the middle high-impedance line. As the discussion in Section 3, the back-to-back C-shaped thin slot is good for high frequency and wide-band suppression, while the triple C-shaped thin slot is suitable for low frequency and narrow-band suppression. For the triple C-shaped thin slot, the outer C-shaped thin slot provides a transmission zero at 4.32 GHz and is used to improve the cut-off response while the middle C-shaped thin slot is used to suppress the narrow-band passband at 9.13 GHz of the conventional SI-LPF. The inner thin slot has a transmission zero at 12 GHz and helps suppress the spurious passband around 12.25 GHz. By (3), the total equivalent inductance of the triple C-shaped thin slot is $L_{eq} = 3.0784$ nH, and the optimized high impedance line of $l_h = 6.65$ mm is used to realize the rest inductance of $L_{con\_3} - 3.0784 = 4.8216$ nH. On

the other hand, the outer two back-to-back C-shaped thin slots are designed with the different lengths to suppress the spurious passband around 12.25 GHz. The left and the right back-to-back C-shaped thin slots are setting to suppress the signal at 11.025 GHz and 12.95 GHz, respectively. Refer to Figure 3(b), the dimensions of the left back-

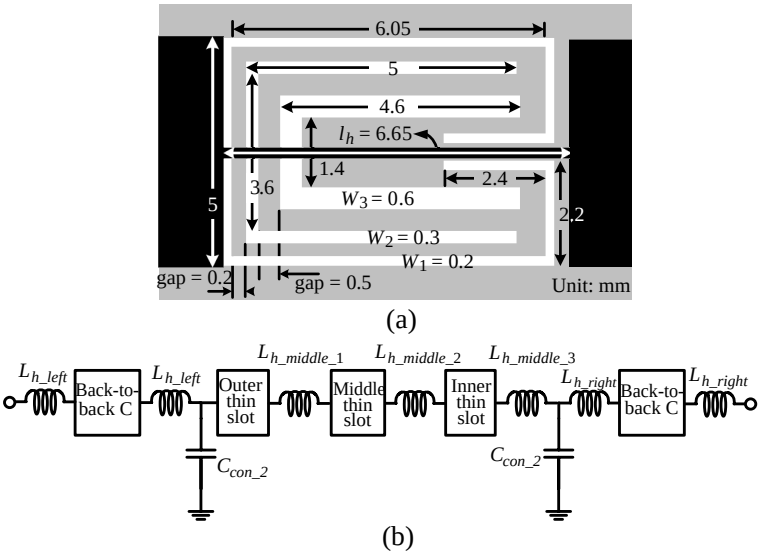

Figure 8. (a) The dimensions of the middle triple C-shaped thin slots, and (b) the equivalent circuit of the proposed SI-LPF.

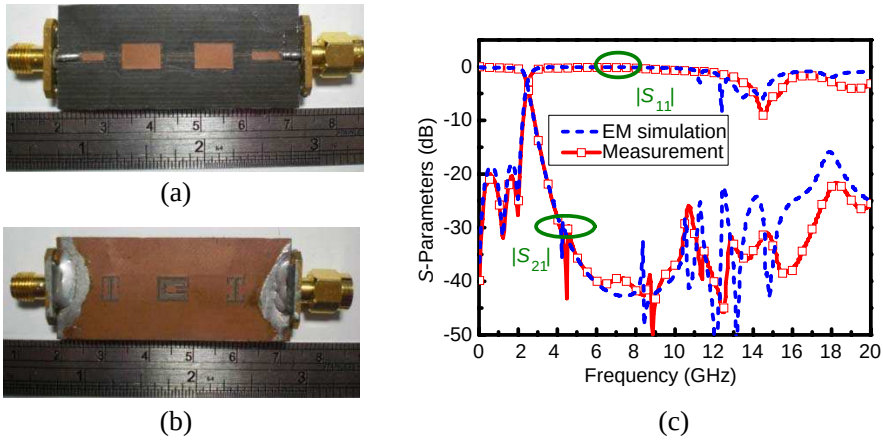

Figure 9. The SI-LPF with C-shaped thin slots, (a) top view, and (b) bottom view, and (c) simulated and measured results.

to-back C-shaped thin slot are: $l = 5\,\text{mm}$, $W = 3.7$ mm, $l_{sa} = 1.89\,\text{mm}$, $W_{sa} = 0.35\,\text{mm}$, and gap $= 0.2\,\text{mm}$. The right back-to-back C-shaped slot has the same dimension as that of the left one except for $l_{sa} = 1.05\,\text{mm}$. By (3), the total equivalent inductance of the left and the right back-to-back C-shaped thin slot is $L_{eq} = 1.6611\,\text{nH}$ and $L_{eq} = 1.5253\,\text{nH}$, respectively.

Thus, the optimized the high impedance microstrip lines of $l_h = 3.8\,\text{mm}$ (left) and $l_h = 3.9\,\text{mm}$ (right) are used to realize the respective rest inductance. Again, the dimensions of the low impedance lines are the same as the conventional one. Figure 8(b) shows the equivalent circuit model of the proposed SI-LPF where the L_{h_left} represents half of the inductance of the left high impedance microstirp line, L_{h_right} is half of the inductance of the right high impedance microstirp line, $L_{h\_middle\_1}$ is the inductance of the high impedance microstirp line between the outer thin slot and middle thin slot, $L_{h\_middle\_2}$ is the inductance of the high impedance microstirp line between the middle thin slot and inner thin slot, and $L_{h\_middle\_3}$ is the inductance of the

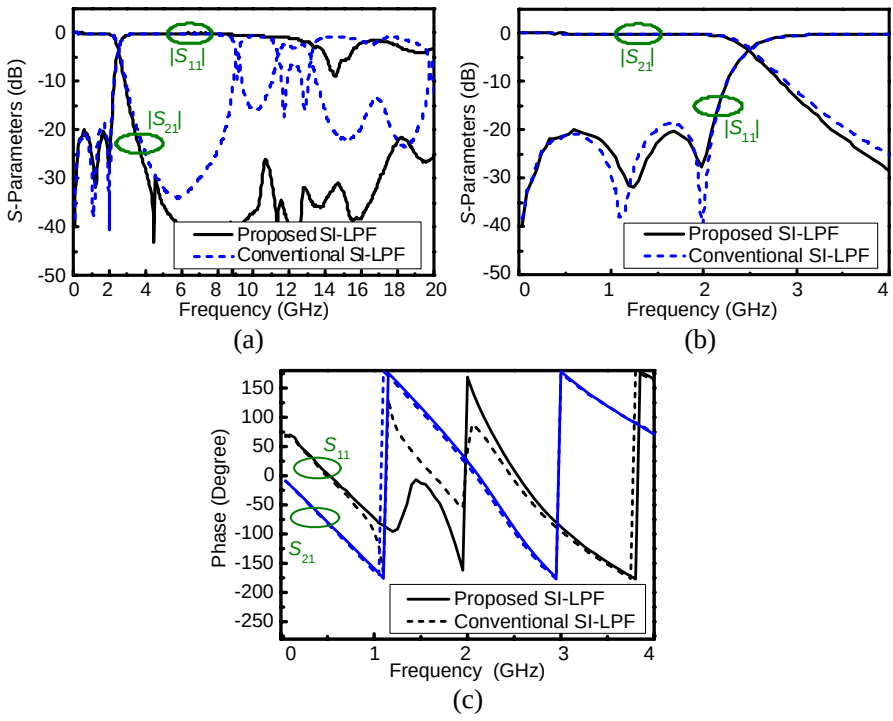

Figure 10. (a) Measured results of convention and proposed SI-LPF, and (b) comparison with conventional SI-LPF, and (c) phase in passband.

high impedance microstirp line between the inner thin slot and low impedance microstirp line.

Figure 9(a) and Figure 9(b) show the photographs of the proposed SI-LPF, and its size is 30.75 mm × 5 mm. The performances of the proposed SI-LPF are shown in Figure 9(c) including EM simulated and measured results of the proposed SI-LPF. From the measured results, the insertion loss in passband is less than 0.3 dB, and the return loss is greater than 20 dB. The rejection is better than 25 dB from 3.7 GHz to 17.7 GHz. Figure 10 compares the measured results of the conventional and the proposed SI-LPFs. With the same passband response, it is

Table 2. Summaries and comparisons of LPFs.

Ref.	f_c (GHz)	Size ($\lambda_g \times \lambda_g$)	SR (%)	Suppression level (GHz@dB)	RS-BW (%)	Pole
[1]	2.5	0.16 × 0.16	45.31	4-14@20 dB	133.63@20 dB	5
[2]	2.14	0.12 × 0.19	38.6	2.8-9.35@20 dB	128.01@20 dB	-
[3]	1.8	0.13 × 0.15	28.21	2.25-7.26@15 dB	123.96@15 dB	3
[5]	5.2	0.76 × 0.46	95.9	5.5-14@20 dB	96.8@20 dB	9
[8]	3.75	0.41 × 0.34	90	4.25-15.9@20 dB	141.72@20 dB	-
[10]	2.4	0.22 × 0.25	74.55	2.7-15@10 dB	193.27@10 dB	-
[11]	2.37	0.18 × 0.31	74.91	4.4-10@25 dB	84.42@25 dB	5
[12]	2.5	0.3 × 0.247	81	2.58-7.5@20 dB	111.8@20 dB	5
[13]	3	0.11 × 0.35	63.64	5-10@30 dB	70.71@30 dB	5
[14]	2.4	0.19 × 0.26	71.65	2.95-8.25@20 dB	107.43@20 dB	5
[15]	2.25	0.26 × 0.52	89.64	2.4-5.5@33 dB[#1]	-	7
[16]	2.53[#2]	0.18 × 0.3	74	2.9-12@20 dB	154@20 dB	7
Conven-tional SI-LPF	2	0.05 × 0.37	24.3	3.07-8.77@15 dB	109.85@15 dB	5
This work	2	0.05 × 0.28	-	3.4-20@20 dB 3.7-17.7@25 dB 3.9-10.5@30 dB	201.30@20 dB 173@25 dB 103.14@30 dB	5

[#1] The measured results are only shown from 2.4 to 5.5 GHz.

[#2] An initial guess gives the cutoff frequency of 2.53 GHz.

clear that the proposed filter achieves a better cut-off rate and a deeper suppression level. Furthermore, the proposed filter also shows a 24.3% size reduction.

For comparison, Table 2 summaries some LPFs, where the circuit sizes have been transformed from the physical area into the effective area. It should be noted that the guided wavelength λ_g is at the cutoff frequency for the corresponding LPFs. The size reduction (SR) is defined as

$$SR = \frac{[Size\ in\ ref.] - [Size\ in\ this\ work]}{[Size\ in\ ref.]}$$

and given a suppression level, the relative stopband bandwidth (RSBW) is given by

$$RS - BW = \frac{stopband\ bandwidth}{stopband\ center\ frequency}$$

From Table 2, one can clearly observe the proposed SI-LPF not only has the small circuit size but also achieves the widest stopband bandwidth than those of others.

6. CONCLUSION

Compact SI-LPFs with ultra-wide stopband by employing thin slots have been presented. The thin slots have features of providing equivalent inductance in the passband and transmission zeros at the stopband. These in turn introduce the advantages of compactness, relaxed fabrication tolerance, and better stopband rejection level. In comparison the conventional SI-LPF and some previously published LPF, the proposed one has a compact size and deep stopband rejection

ACKNOWLEDGMENT

This work was supported in part by National Science Council, Taiwan, under contract No. NSC 100-2221-E-008-113 and NSC 100-2221-E-008-114

REFERENCES

1. Kim, I. S. and S. W. Yun, "Compact LPF using asymmetrical microstrip step discontinuity for harmonic suppression," *Electron. Lett.,* Vol. 41, No. 16, 41–42, Aug. 2005.

2. Li, L. and Z.-F. Li, "Compact quasi-elliptic lowpass filter using symmetric rectangular coupled capacitors," *Electron. Lett.,* Vol. 44, No. 2, 124–125, Jan. 2008.
3. He, Q. and C. Liu, "A novel low-pass filter with an embedded band-stop structure for improved stop-band characteristics," *IEEE Microw. Wireless Compon. Lett.*, Vol. 19, No. 10, 629–631, Oct. 2009.
4. Tu, W.-H. and K. Chang, "Microstrip elliptic-function low-pass filters using distributed elements or slotted ground structure," *IEEE Trans. Microw Theory Tech.*, Vol. 54, No. 10, 3786–3792, Oct. 2006.
5. Wang, L., H.-C. Yang, and Y. Li, "Design of compact microstrip low-pass filter with ultra-wide stopband using sirs," *Progress In Electromagnetics Research Letters*, Vol. 18, 179–186, 2010.
6. Yang, M., J. Xu, Q. Zhao, L. Peng, and G. Li, "Compact, broad-stopband lowpass filters using sirs-loaded circular hairpin resonators," *Progress In Electromagnetics Research*, Vol. 102, 95–106, 2010.
7. Weng, L. H., Y.-C. Guo, X.-W. Shi, and X.-Q. Chen, "An overview on defected ground structure," *Progress In Electromagnetics Research B*, Vol. 7, 173–189, 2008.
8. Chen, H.-J., T.-H. Huang, C.-S. Chang, L.-S. Chen, N.-F. Wang, Y.-H. Wang, and M.-P. Houng, "A novel cross-shape DGS applied to design ultra-wide stopband low-pass filters," *IEEE Microw. Wireless Compon. Lett.*, Vol. 16, No. 5, 252–254, May 2006.
9. Al Sharkawy, M. H., D. Abd El-Aziz, and E. G. Mahmoud, "A miniaturized lowpass/bandpass filter using double arrow head defected ground structure with centered etched ellipse," *Progress In Electromagnetics Research Letters*, Vol. 24, 99–107, 2011.
10. Wei, F., L. Chen, X.-W. Shi, Q.-L. Huang, and X.-H. Wang, "Compact lowpass filter with wide stop-band using coupled-line hairpin unit," *Electron. Lett.,* Vol. 46, No. 1, 88–90, Jan. 2010.
11. Lim, J.-S., C.-S. Kim, D. Ahn, Y.-C. Jeong, and S. Nam, "Design of low-pass filters using defected ground structure," *IEEE Trans. Microw. Theory Tech.*, Vol. 53, No. 8, 2539–2545, Aug. 2005.
12. Xi, D., Y.-Z. Yin, L.-H. Wen, Y. Mo, and Y. Wang, "A compact low-pass filter with sharp cutoff and low insertion loss characteristic using novel defected ground structure," *Progress In Electromagnetics Research Letters*, Vol. 17, 133–143, 2010.
13. Balalem, A., A. R. Ali, J. Machac, and A. Omar, "Quasi-elliptic microstrip low-pass filters using an interdigital DGS slot,"

IEEE Microw. Wireless Compon. Lett., Vol. 17, No. 8, 586–588, Aug. 2007.

14. Yang, J. and W. Wu, "Compact elliptic-function low-pass filter using defected ground structure," *IEEE Microw. Wireless Compon. Lett.*, Vol. 18, No. 9, 578–580, Sept. 2008.
15. Chen, J., Z.-B. Weng, Y.-C. Jiao, and F.-S. Zhang, "Lowpass filter design of Hilbert curve ring defected ground structure," *Progress In Electromagnetics Research*, Vol. 70, 269–280, 2007.
16. Wang, C.-J. and T. H. Lin, "A multi-band meandered slotted-groundplane resonator and its application of lowpass filter," *Progress In Electromagnetics Research*, Vol. 120, 249–262, 2011.
17. Ahn, D., J.-S. Park, C.-S. Kim, J. Kim, Y. Qian, and T. Itoh, "A design of the low-pass filter using the novel microstrip defected ground structure," *IEEE Trans. Microw Theory Tech.*, Vol. 49, No. 1, 86–93, Jan. 2001.
18. Hong, J.-S. and B. M. Karyamapudi, "A general circuit model for defected ground structures in planar transmission lines," *IEEE Microw. Wireless Compon. Lett.*, Vol. 15, No. 10, 706–708, Oct. 2005.
19. IE3D Version 11.1, Zeland Software Inc., Dec. 2005.
20. Hong, J.-S. and M. J. Lancaster, *Microstrip Filters for RF/Microwave Applications*, Wiley, New York, 2001.